



Antimicrobial thin-film composite polyamide nanofiltration membrane with high desalination and flux performance manufactured through a novel UV light driven photoreduction method that generates dispersed silver nanoparticles

Shanshan Dong^a, Xinping Zhang^a, Ying Xiong^{b,*}, Xuhui Mao^c, Xin Wu^a, Na Li^a, Shengyun Yang^d, Helin Hua^{a,*}

^aKey Laboratory of Jiangxi Province for Persistent Pollutants Control and Resources Recycle, School of Environmental and Chemical Engineering, Nanchang Hangkong University, 696 Fenghe South Avenue, Nanchang 330063, China, Tel.: +86-791-83953375; Fax: +86-791-83953373; emails: huahelin@nchu.edu.cn (H. Hua), 71048@nchu.edu.cn (S. Dong), 1547618427@qq.com (X. Zhang), 627176514@qq.com (X. Wu), 39013@nchu.edu.cn (N. Li)

^bGuangdong Provincial Key Laboratory of Soil and Groundwater Pollution Control, School of Environmental Science and Engineering, Southern University of Science and Technology, Shenzhen 518055, China, Tel.: +86-791-83953375; Fax: +86-791-83953373; email: xiongy@sustech.edu.cn

^cSchool of Resource and Environmental Sciences, Wuhan University, Wuhan 430079, China, email: clab@whu.edu.cn

^dGuangdong Weiqing Environmental Engineering Company, Zhongshan 528437, China, email: shengyun1998@163.com

Received 23 July 2022; Accepted 2 December 2022

ABSTRACT

Incorporation of antibacterial Ag nanoparticles (AgNPs) is thought to effectively control the biofouling of the thin-film composite (TFC) nanofiltration membrane for efficient desalination. In this study, a UV photoreduction reaction was employed for the first time to introduce AgNPs into the separation active layer of nanofiltration membrane to avoid the normal membrane blockage by conventional blending method. The additional merit of the UV irradiation was the partial oxidation of membrane surface, which provides more hydrophilic groups. Compared with the pristine TFC membrane, the AgNPs-loaded (TFC-Ag) membrane possessed much better hydrophilic property (with an increase in pure water flux by 99%), and maintained high salt rejection efficiency. The high antibacterial performance of the TFC-Ag membrane was demonstrated by the 96% inhibition efficiency to *Escherichia coli*. Besides, the TFC-Ag membrane only showed a trace amount of Ag⁺ release in the static and dynamic tests, showing great stability for water treatment. This study provides an innovative strategy for the *in-situ* production of metallic nanoparticles to modify the nanofiltration membrane and to improve its water flux and anti-bacterial performance.

Keywords: Nanofiltration membrane; Polyamide; UV irradiation; Ag nanoparticles; Membrane biofouling

1. Introduction

Water contamination and scarcity has been the serious challenge to the human development and consequently drawn great attention. Membrane separation is one of the

most promising technologies to handle the water contamination and shortage due to the high efficiency, low-cost and environmental friendless. Nanofiltration membrane plays an important role in high-quality water production, but the membrane fouling was the major problem that has

* Corresponding authors.

not been completely resolved [1–7]. Biological pollution was thought as one of the most influential factors on the performance of membrane, which reduced the water flux of membrane, changed the retention characteristic of membrane, and shortened the service life of membrane [4–6,8–10]. Therefore, it is necessary to find effective methods to reduce the biological pollution of the membrane.

Introducing antimicrobial nanomaterials in membrane fabrication could improve membrane hydrophilicity and reduce biological contamination [11–17]. Due to its strong disinfection capacity and low toxicity to mammalian cells, silver nanoparticle (AgNP) is constantly a research hotspot that has received significant attentions among the antimicrobial nanomaterials. Direct addition of AgNPs in polymer solution is the conventional method to prepare antimicrobial membrane [18–20]. However, serious particle aggregation was observed to result in membrane blockage and decreased membrane permeation performance [21]. Therefore, *in-situ* hybridization method was proposed to generate AgNPs in the formed separation layer of membrane. Jeong et al. [17] prepared thin-film composite (TFC) reverse osmosis membrane with uniformly covered AgNPs via chemically reducing silver ions. Some researchers also prepared AgNPs on the surface of polystyrene membrane by chemical reduction using sodium borohydride [22,23]. However, the current procedure for *in-situ* production of AgNPs is complicated for the preparation of antimicrobial TFC membrane. For example, the grafting reaction of membrane matrix had to be carried out before reduction, otherwise there were no reduction sites to enable the close connection of AgNPs with the membrane. Moreover, the use of strong reducing agent sodium borohydride often caused an uncontrollable reaction rate that intensified the aggregation of AgNPs. Therefore, facile and green methods for preparing AgNPs coated membrane are still highly desired.

Photoreduction is an alternative method that allows to obtain metal nanoparticles [24,25]. Scaiano et al. [24] used a variety of photochemical reduction systems to prepare gold, silver, copper, and cobalt metal nanoparticles. Stampelcoskie and Scaiano [25] used LED light to irradiate metal precursors and successfully prepared AgNPs with various shapes and sizes by changing light wavelength. Their studies showed that, in comparison with the chemical reduction process using reducing reagents, the condition of photoreduction was relatively mild, and the reaction rate and material structure could be regulated by controlling light radiation [24,25]. Considering the merits of the photoreduction, in the present study, the photoreduction method is explored for the first time for preparing a AgNPs loaded thin-film composite (TFC-Ag) membrane.

In this study, an ultra-thin separation layer was first prepared onto a polysulfone (PSF) membrane by an interfacial polymerization method, and then the as-prepared TFC membrane was immersed in AgNO_3 solution to achieve the dispersion of Ag^+ in the membrane. The followed UV photoreduction process allowed the production of the TFC-Ag membrane. The preparation procedure is schematically illustrated in Fig. 1. Under the UV irradiation, the photoinitiator benzophenone (BP) was excited to produce reducing radicals, which reduced Ag^+ ions to AgNPs on the surface

of the membrane. The aim of this study is to explore the feasibility of the photoreduction method for the synthesis of AgNPs loaded membrane. The properties of the obtained TFC-Ag membrane were evaluated, and its performance for nanofiltration process, especially for biofouling resistance was studied. This study reveals that the photoreduction process is a favorable method that allows to prepare composite membrane material with favorable property for water treatment.

2. Materials and methods

2.1. Materials

Polysulfone (PSF, Udel P-3500 LCD MB7, American), N,N-dimethylacetamide (DMAc), polyethylene glycol 400 (PEG400), benzophenone (BP), AgNO_3 , Na_2SO_4 , MgCl_2 , CaCl_2 and NaCl were purchased from the Xilong Scientific Co., Ltd., China. Ethanol, hydro piperazine (PIP > 98%) and para-phenyltrimethyl chloride (TMC > 99%) were bought from the Shanghai Maclin Biochemical Technology Co., Ltd., China. *Escherichia coli* 25922 (*E. coli*) and Bovine Serum Albumin (BSA) were obtained from the Shanghai Luwei Technology Co., Ltd., China. All reagents used in this research were analytical grade unless otherwise indicated.

2.2. Preparation of membrane materials

TFC membrane was lab-made according to the study of Xie et al. [26] and Liu et al. [27]. Briefly, PSF was dissolved into DMAc solution and PEG400 was added as the additive. The casting solution was preserved at 70°C. The prepared PSF solution was cast on a polyethylene terephthalate (PET) fiber mesh (the support layer), then the PSF membrane was obtained by a liquid–solid phase transformation method. For the preparation of TFC membrane, the as-prepared PSF membrane was fixed in a special film-making frame. PIP solution (0.1 wt.%) was poured into a rectangular frame, and was kept in contact with the surface of PSF membrane for 15 min. Then, the membrane was taken out to remove the extra PIP solution. Afterwards, TMC solution (0.1 wt.%) was poured onto the PSF membrane surface with PIP to perform interfacial polymerization reaction. The reaction time was set at 90 s. The resulting membrane was washed with hexane and then baked at 60°C for 15 min. As such, a dense separation layer was formed on the surface of PSF membrane, and the obtained material was TFC membrane.

For the preparation of TFC-Ag membrane, the photoreduction solution was prepared by fully mixing silver nitrate (AgNO_3), photoinitiator benzophenone (BP) and ethanol. The prepared TFC membrane was immersed in the photoreduction solution for 1 h to ensure that the solution fully infiltrated the membrane. The impregnated membrane was then taken out and put into the photoreduction reactor. The reactor, with a transparent quartz window on the top plate, allows the UV irradiation from a 365 nm UV lamp. The pressure of the reactor was pumped to -20 KPa to evacuate the air, and the UV lamp was then turned on to start the photoreduction process. After irradiation for a certain period, the obtained TFC-Ag membrane was taken out and washed with deionized (DI) water to completely remove the residual solute, solvent, and the loosely connected metal

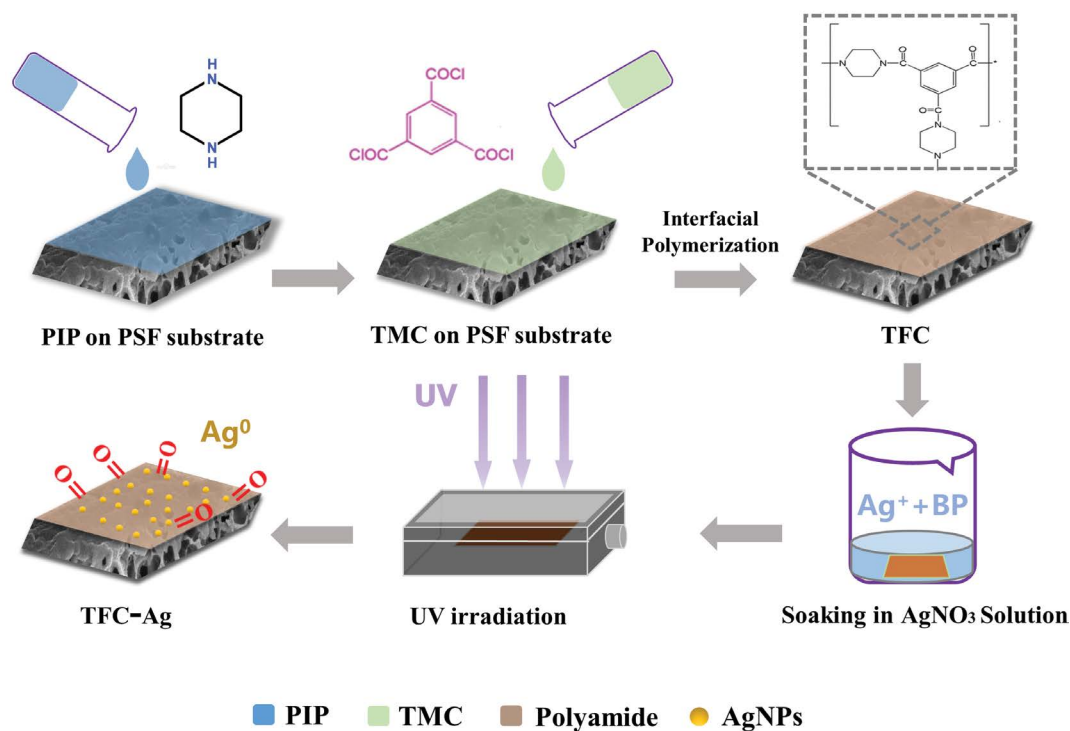


Fig. 1. Schematic diagram of the procedure for preparation of TFC-Ag composite membrane, and the photoreduction reaction for the *in-situ* synthesis of AgNPs under UV irradiation.

particles. The obtained TFC-Ag membrane was stored in DI water for further analysis. If not specified elsewhere, the TFC-Ag membrane refers to the material prepared with 20 mM AgNO_3 .

2.3. Analytical and characterization methods

The phases and chemical compositions of the membrane materials were studied by means of X-ray diffraction (XRD; AXS-D8, Bruker, Switzerland) and Fourier-transform infrared spectroscopy (FTIR; VERTEX70, Bruker, Switzerland). The morphology of surface and cross-section of membranes were analyzed by scanning electron microscopy (SEM; Supra 55, Sapphire, Germany) and transmission electron microscopy (TEM; JEM-1230, Jeol, Japan). In addition, the membranes incubated with *E. coli* was also characterized by SEM analysis to observe the bacterial morphology on the membrane surface. The pretreated procedures of SEM analysis for bacterial samples were as follows: the bacterial samples were first fixed with 2.5% (v/v) glutaraldehyde at 4°C for 5 h, then dehydrated and washed with gradient ethanol solutions for 15 min each time, finally dried in air. The surface roughness of membrane was measured with atomic force microscopy (AFM; MFP-3D infinity, Asylum Research, English). X-ray photoelectron spectroscopy (XPS) measurements were performed using the Axis Ultra DLD system from Kratos Analytical Ltd. with monochromatic Al $K\alpha$ radiation and a pass energy of 20 eV. Ag loading density was obtained by analyzing the dissolving amount of Ag^+ from the membrane using 2-(3,5-dibromo-2-pyridylazo)-5-diethylaminophenol (3,5-Br₂-PADAP)

spectrophotometric method [28]. The membranes sample was first immersed in 3 mL of nitric acid solution (v:v = 1:3) for 3 h, and then sonicated for 15 min to ensure the efficient dissolution of the loaded AgNPs. Ag loading mass was obtained by analyzing the leached Ag^+ in the acid solution. Dividing Ag loading mass by membrane surface area was the Ag loading density ($\mu\text{g}/\text{cm}^2$). The detailed procedure of the spectrophotometric method for Ag^+ analysis is given in S1 in the Supporting information.

2.4. Hydrophilicity and separation performance of membrane

The hydrophilicity of membrane was evaluated by a contact angle meter (SDC-100, Dongguan Shengding Precision Instrument Co., Ltd., China). The membrane separation performance was determined by a flat membrane cross-flow filtration equipment (Fumei, China). Permeation flux refers to the volume of permeate passing through a unit membrane area within a unit time period during the membrane separation process. The calculation formula is shown as below:

$$J = \frac{V \times A}{\Delta t} \quad (1)$$

where J is the membrane permeation flux ($\text{L}/\text{m}^2\cdot\text{h}$); V is the volume of permeate (L); A is the filter membrane area and Δt is the testing time. The rejection efficiency refers to the percentage of solute in the feed liquid removed by the separation membrane system. The calculation formula is shown as Eq. (2):

$$R = \left(1 - \frac{C_p}{C_f} \right) \times 100\% \quad (2)$$

where R is the membrane rejection efficiency (%); C_p is the solute concentration in permeate (mg/L); and C_f is the solute concentration in feed liquid (mg/L).

2.5. Antibacterial performance and stability of membrane

Gram-negative *E. coli* (ATCC25922) was adopted as the model microorganism for assessing the antibacterial performance of membrane by the inhibition zone method and plate counting method. For the inhibition zone method, membrane samples were cut into circles of 6 mm in diameter and sterilized by UV light irradiation for 30 min. Then, 100 μ L of the *E. coli* suspension (10^4 CFU/mL) was uniformly coated on a culture plate, and covered with a TFC membrane at 37°C for 24 h. For the plate counting method, membrane samples were cut into circles of 2 cm in diameter and sterilized by UV light irradiation for 30 min. 400 μ L of the *E. coli* suspension (10^5 CFU/mL) was dropped in a sterilized petri dish and then covered with an obtained TFC membrane piece to form an *E. coli* sandwich. The *E. coli* sandwich was cultured at 37°C for 2 h and washed by 10 mL of phosphate buffer solution (PBS). 100 μ L of such eluent was evenly coated on the culture plates, and cultured at 37°C for 24 h. Then, the colony number on the surface of solid medium was counted. The colony number of the sample was recorded as $N_{A'}$ and the blank control colony number was recorded as N_B . Specifically, a petri dish without membrane sample was taken and performed the same operation as the blank control. The antibacterial efficiency η of membrane was calculated according to Eq. (3):

$$\eta = \frac{N_B - N_{A'}}{N_B} \times 100\% \quad (3)$$

The static soaking and dynamic filtering tests were carried out to evaluate the stability of the TFC-Ag membrane. For the static test, the TFC-Ag membrane samples were cut into 4 cm \times 6 cm size and immersed in 2 L of DI water, and the released Ag^+ ion was measured each day. In the dynamic test, the TFC-Ag membrane was placed in a flat membrane cross-flow filtration equipment. Under the operating condition of 0.6 MPa pressure and testing temperature 25°C \pm 0.5°C, the filter equipment was operated using DI water and the resulting Ag^+ releasing amount was measured. The dynamic test was repeated 10 times.

3. Results and discussion

3.1. Structural and morphological characteristics of membranes

Fig. 2a shows the XRD spectra of the TFC and TFC-Ag membranes. The broad peaks between 15° to 30° are assigned to the polysulfone in the TFC membrane. For the TFC-Ag membrane, the diffraction peaks of 37.85°, 43.97°, 64.42° and 77.40° correspond to the crystal planes of (1 1 1), (2 0 0), (2 2 0) and (3 1 1) of zero valent silver particles [29], respectively. The presence of the signal of Ag indicated their

successful loading onto the TFC membrane. Meanwhile, the TFC and TFC-Ag membrane both had the polysulfone peaks with the same intensity, which suggests that the introduction of AgNPs did not destroy the structure of the TFC membrane. According to the reported studies, AgNPs with different size affected the structural characteristics of the pristine membrane in different ways [20]. Mollahosseini et al. [20] prepared a TFC-Ag membrane using AgNPs-containing casting solution, and it was found that AgNPs with an average diameter less than 30 nm decreased the peak intensity of the PSF membrane, while AgNPs with an average diameter of 70 nm did not [30]. Therefore, further analysis was carried out to determine the content and size of the incorporated AgNPs.

The XPS scan spectra of the TFC and TFC-Ag membranes are shown in Fig. 2b. The signal of Ag 3d (Fig. 2b) and deconvolution of Ag 3d XPS spectrum in Fig. S1 in the SM confirmed that zero-valent AgNPs were successfully loaded in the TFC-Ag membrane. The binding energies of the C and N are shown in Fig. 2c and d. In Fig. 2c, the peak of the C 1s could be de-convoluted into three peaks located at 288.2, 286.2, and 284.8 eV, assignable to C=O, C–N and C–C, respectively [31]. The deconvolution of the N 1s spectra identified peaks located at 401.7 and 400.0 eV (Fig. 2d), attributing to N–H and N–C=O, respectively [32]. After UV irradiation, the N 1s and C 1s spectra of the TFC-Ag membrane exhibited obvious changes compared to the pristine membrane. It was found that the C 1s spectra of the TFC shifted to higher binding energies, which is ascribed to the conversion of C–C to C–N and C=O. The N 1s spectra shifted to lower binding energies, which is explained by the conversion of N–H to O=C–N. These observations reveal that, along with the *in-situ* formation of AgNPs, the active layer of the TFC membrane experienced a partial oxidative process. In other words, the ratio of reducing groups (C–N, C–C and N–H) decreased, while the ratio of oxidized groups (C=O and N–C=O) increased after UV irradiation. The oxidation of these reducing groups under UV irradiation accords with the reported studies [24,33,34]. The anticipated benefit of the presence of strongly polar C=O groups is that they could increase the hydrophilicity of the TFC-Ag membrane. Its hydrophilicity is further studied in the subsequent section of this study.

Fig. 3a–c present the SEM images of the PSF, TFC and TFC-Ag membranes, and the three membrane samples show different characteristics. Some randomly distributed pores were observed for the PSF membrane, while TFC membrane surface was dense without large pores. Uniformly distributed AgNPs were observed on the surface of the TFC-Ag membrane. The SEM images of cross-section of the three membranes are shown in Fig. 3d–f. Compared to the PSF and TFC membrane, the TFC-Ag membrane had no significant changes in the cross-section which indicates the loading of AgNPs did not destroy the porous structure of the TFC membrane. Through the energy-dispersive X-ray spectroscopy (EDS) scanning of the cross-section of the TFC-Ag membrane, the distributions of each element in the membrane are given in the enlarged inset, in which the atomic content of Ag was around 0.06%. Owing to the fact that EDS is a semi-quantitative technique for the analysis of the surface composition of the sample, we then used 3,5-Br2-PADAP spectrophotometric

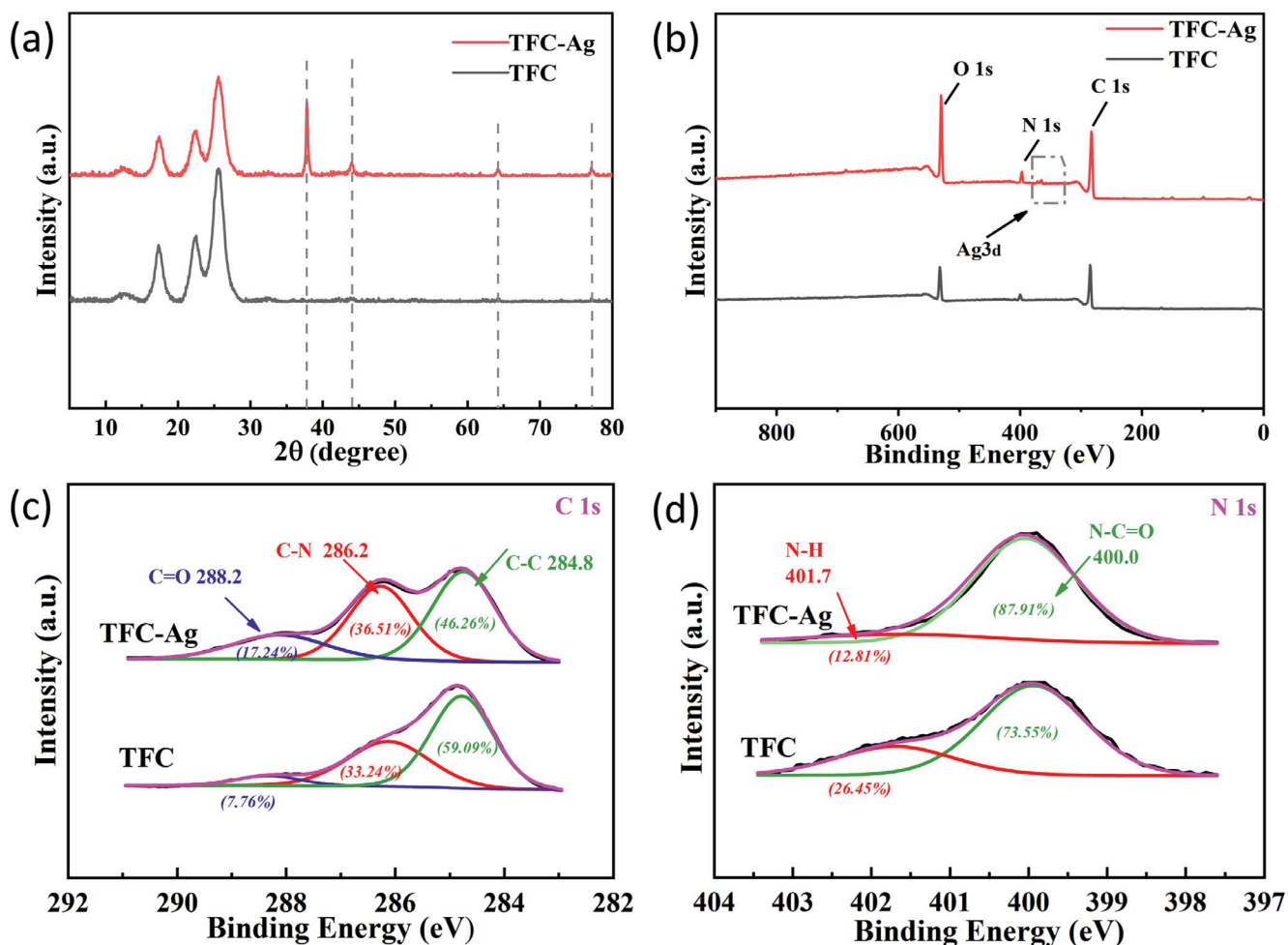


Fig. 2. (a) XRD patterns and (b) XPS spectra of the TFC and TFC-Ag membranes. (c,d) C 1s and N 1s XPS spectra of the TFC and TFC-Ag membranes.

method [28] to quantitatively analyze the Ag loading density. The Ag loading densities of TFC-Ag membranes are shown in Fig. S2. With the increase of AgNO_3 concentration from 20 to 100 mM, the Ag loading density increased from 15.4 to 53.8 $\mu\text{g}/\text{cm}^2$. The TEM image (Fig. 3h) of the TFC-Ag membrane shows that the thickness of polyamide separation layer is about 168 nm, and AgNPs dispersed in the separation layer. The TEM image also reveals that the diameters of the incorporated AgNPs are in the range of 12–60 nm, and most AgNPs possessed the diameter of less than 24 nm. Combining with the results of XRD, SEM and TEM, it suggests that the AgNPs with average diameter less than 30 nm would not destroy the structure of the TFC membrane, which was also confirmed by the FTIR spectra (Fig. S3). The result was different with the reported study [20], in which the *ex-situ* loaded AgNPs of 30 nm on PSF-based membrane resulted in a decreased PSF XRD peak and consequently affected PSF membrane structure. The TEM results suggest that the *in-situ* formation of AgNPs is superior to that of direct introduction of AgNPs because no severe aggregation of nanoparticles was found.

It is also interesting to compare this *in-situ* photoreduction method with biogenic method, another pioneering

strategy to achieve a good dispersion of AgNPs [35–37]. The preparation of biogenic AgNPs used bacteria to reduce and cap silver ions. The separation of AgNPs from bacteria faced complicated procedures of purification, such as the addition of NaOH and multistage centrifugation. The biogenic AgNPs-modified composite nanofiltration membranes were synthesized through two methods: (1) introducing the biogenic AgNPs in interfacial polymerization process [35] and (2) TFC surface modification by thiol [36]. The first method was found to relatively reduce the extent of interfacial polymerization degree, which harmed desalination efficiency. The second method would bring a concern about the stability of the thiol bonding to substrate membrane surface. And the water flux enhancement of thiol assisted AgNP-loading-TFC membrane seemed to mainly originate from the thiol modification rather than the introduction of biogenic AgNPs. A recent work that synthesized biogenic AgNPs-modified forward osmosis membranes with enhanced water flux [37] is difficult to be compared with our TFC-Ag nanofiltration membrane which works in pressure-driven mode. In our study, the *in-situ* photoreduction process can be easily tuned in spatial and temporal scale to achieve high level of AgNPs dispersion without

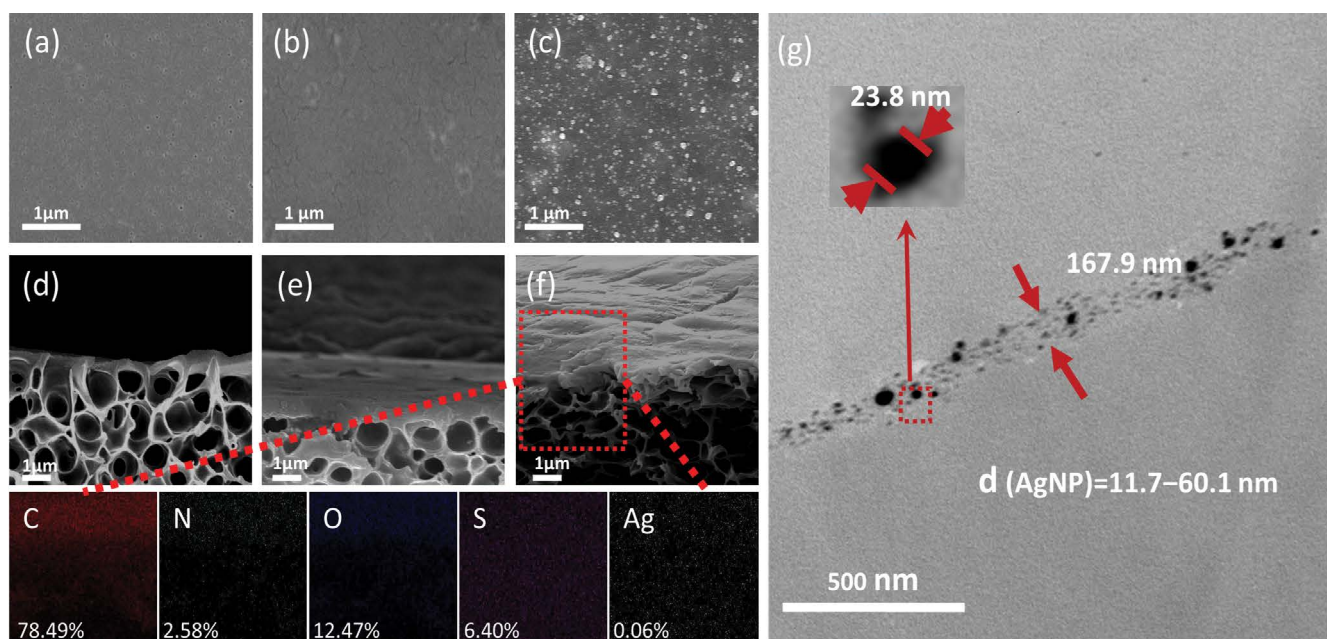


Fig. 3. SEM images of membrane surfaces and cross-sections: (a,d) PSF, (b,e) TFC, (c,f) TFC-Ag and EDS of C, N, O, S, and Ag. (g) TEM image of the TFC-Ag membrane.

worrying about the damage of membrane skeleton construction by AgNPs loading. To some extent, the blockage of membrane channel by high AgNPs loading amount should still be avoided for the *in-situ* photoreduction method.

AFM was used to probe the roughness of the membrane samples. Fig. 4 shows the 2D and 3D images of the pristine PSF, TFC and TFC-Ag membranes. The PSF membrane had a smooth surface and the lowest R_q (1.712 nm) and R_a (1.345 nm). With the formation of polyamide dense separation layer and the introduction of AgNPs in the pristine membrane, the roughness of TFC membrane ($R_q = 6.712$ nm, $R_a = 5.348$ nm) and TFC-Ag membrane ($R_q = 8.247$ nm, $R_a = 6.492$ nm) gradually increased. The change in roughness proves the successful loading of the AgNPs onto the surface of TFC membrane.

3.2. Effect of preparation condition on the separation performance of TFC-Ag membrane

The separation performance of composite nanofiltration membrane is determined by its chemical composition and the preparation condition. Fig. 5a shows the effect of UV irradiation time on water flux and Na_2SO_4 rejection performance of TFC-Ag membrane. When the irradiation time increased from 30 to 90 min, the water flux increased and the salt rejection decreased slightly. When the irradiation time was 90 min, the TFC-Ag membrane offered the largest water flux 85.79 L/m²·h and the salt rejection was 94.14%. Compared to the water flux (43.15 L/m²·h) and the salt rejection (97.83%) of the TFC membrane, the water flux of TFC-Ag membrane increased by 99%, while the salt rejection was slightly reduced. When the irradiation time increased to 120 min, the water flux no longer increased. With the time increasing, more AgNPs formed on the TFC-Ag membrane,

and their aggregation blocked the membrane channels. Therefore, the optimal irradiation time is 90 min.

The water flux and separation performance of the TFC-Ag membranes prepared with different AgNO_3 solutions were tested. In respect to the hydrophilicity of the introduced AgNPs, the salt rejection of all the TFC-Ag membranes was more than 90%, and the water flux was noticeably higher than that of TFC membrane as well. When the AgNO_3 concentration was 20 mM, the flux of TFC-Ag membrane was 84.15 L/m²·h, which was 95% higher than that of TFC membrane (43.15 L/m²·h). It can be noted that the rejection efficiency remained high with the AgNO_3 concentration augmented from 20 to 100 mM, but the water flux of the TFC-Ag membrane decreased to 62.64 L/m²·h (still about 1.5 times of that of TFC membrane). Fig. S2 exhibits the markedly increased AgNPs loading density in the range of 20–100 mM AgNO_3 concentration. The loss of water permeability at the higher AgNO_3 concentration (>20 mM) might be ascribed from the overloading of AgNPs which caused the aggregation of the AgNPs and the resulting blockage of the membrane channels. The declined effective hydrophilic surface area of the nanofillers among the aggregated nanoparticles might also be the reason for the increased contact angle of TFC-Ag membranes (Fig. 5c). This result is consistent with some other reports [23,38,39].

Fig. 5c depicts the change of contact angle with AgNO_3 concentration. Due to the strong hydrophilicity of Ag nanoparticle [19,40,41], the hydrophilicity of TFC-Ag membranes was accordingly improved. When the AgNO_3 concentration was 20 mM, the TFC-Ag20 membrane had the best hydrophilicity among these TFC-Ag membrane samples. The contact angle of TFC-Ag20 membrane decreased from 77.4° to 40.2°. The results of water flux, separation and contact angle indicate that 20 mM AgNO_3 concentration

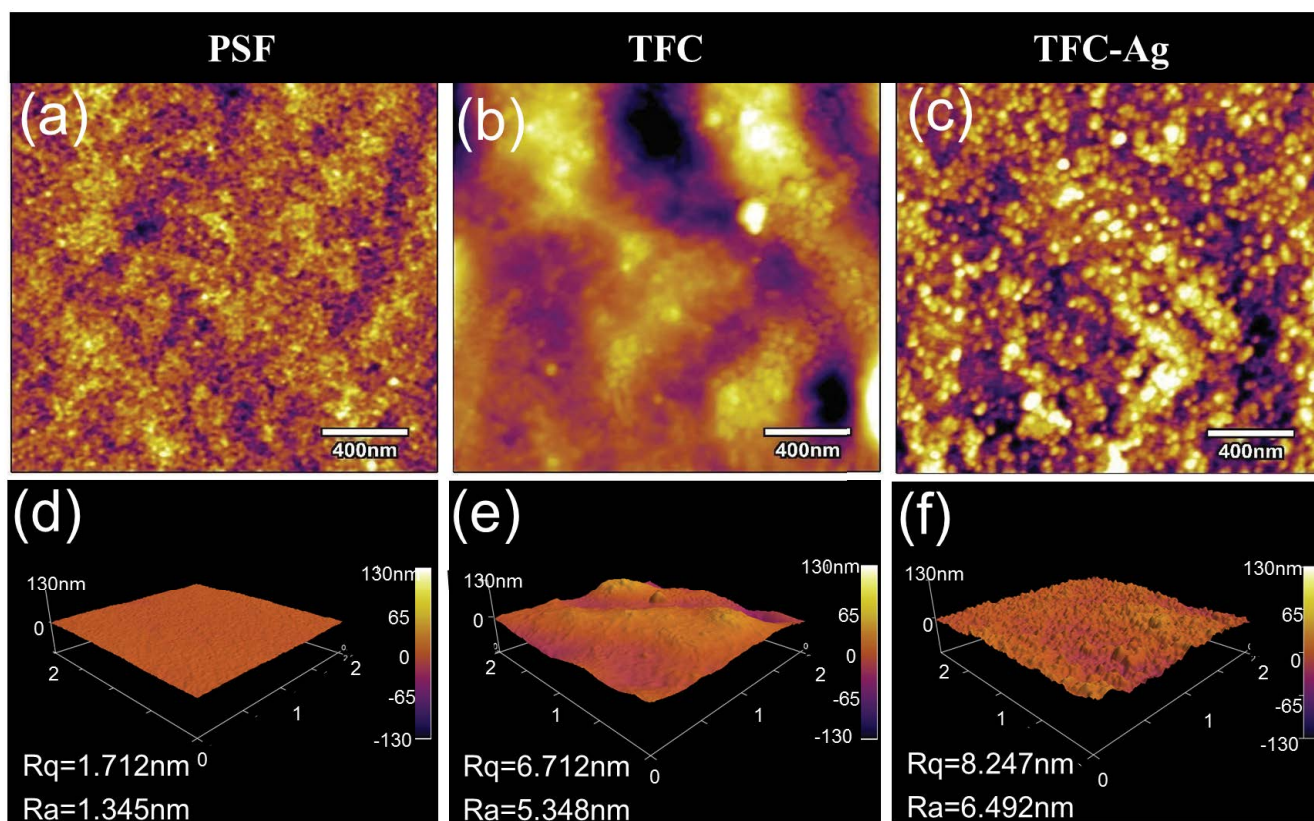


Fig. 4. Surface AFM images of (a,d) PSF, (b,e) TFC and (c,f) TFC-Ag membrane.

allowed the preparation of the TFC-Ag membrane with best hydrophilicity.

3.3. Stability test of AgNPs in the TFC-Ag membrane and water flux

Fig. 6a and b presents the concentration change of Ag^+ ion in static and dynamic experiments. The concentration of Ag^+ ion in water was constantly lower than 0.05 mg/L during the 7 d of immersion (Fig. 6a). In regarding to TFC-Ag20, although 20.7% of AgNPs loss was observed in the first 5-d immersing in water (Fig. 6a), Ag leaching nearly stopped after the 5th day. The observation for the loss of AgNPs is similar with previous researches [37,42]. Dynamic test results (Fig. 6b) show that the released Ag concentrations in filtrate and concentrate both quickly decreased to ~ 0.01 mg/L after 5-cycle running. It means that the releasing rate quickly dropped and stabilized at a low level after 5-cycle running. It can be calculated that only 14.6% of AgNPs loss occurred after 10-cycle running. Therefore, the stability of the as-prepared TFC-Ag membrane is satisfactory.

In the dynamic experiment, the Ag^+ ion concentrations in the filtrate were above 0.05 mg/L in the first to the third operation cycles. Subsequently, the Ag^+ ion concentrations in filtrate was constantly lower than 0.05 mg/L. The Ag^+ ion concentration in the concentrate shows a faster decreasing trend, being less than 0.05 mg/L after 4 cycles. In the Chinese National Standard for Drinking Water Quality (GB 5749-2006), the concentration of detected Ag is

required to be <0.05 mg/L. The World Health Organization (WHO) reported that Ag^+ ions less than 0.1 mg/L is safe to human health [43]. According to these standards, the stability of TFC-Ag membrane could meet its use even in the drinking water treatment. The variation of water flux of the TFC-Ag membrane with running times is indicated in Fig. 6c. Obvious water flux attenuation was observed in the initial three operations, then the water flux stabilized at the level about $65 \text{ L/m}^2\text{-h}$, showing favorable capacity to hold the water flux. In order to compare with other reported Ag-TFC membranes, the water flux was calculated as $10.84 \text{ L/m}^2\text{-h-bar}$ given the operating pressure of 6 bar. Compared with the *in-situ* fabricated Ag-TFN membrane (the water flux as $1.9 \pm 0.1 \text{ L/m}^2\text{-h-bar}$) and the *ex-situ* fabricated Ag-TFN membranes (the water flux as 2.7 to $3.3 \text{ L/m}^2\text{-h-bar}$) [44], the Ag-TFC membrane of this study exhibited excellent water flux. The comparable water flux owed to two reasons: (1) The diameter of AgNPs by UV photoreduction method was mostly less than 24 nm, which enhanced interfacial free volume and did not block the membrane channels; (2) the UV irradiation led to the oxidation of the active separation layer oxidized and increased the hydrophilicity of the Ag-TFC membrane.

3.4. Antibacterial and anti-fouling performance of TFC-Ag membrane

Fig. 7 gives the optical images of colony number on solid agar which had been treated by TFC and TFC-Ag

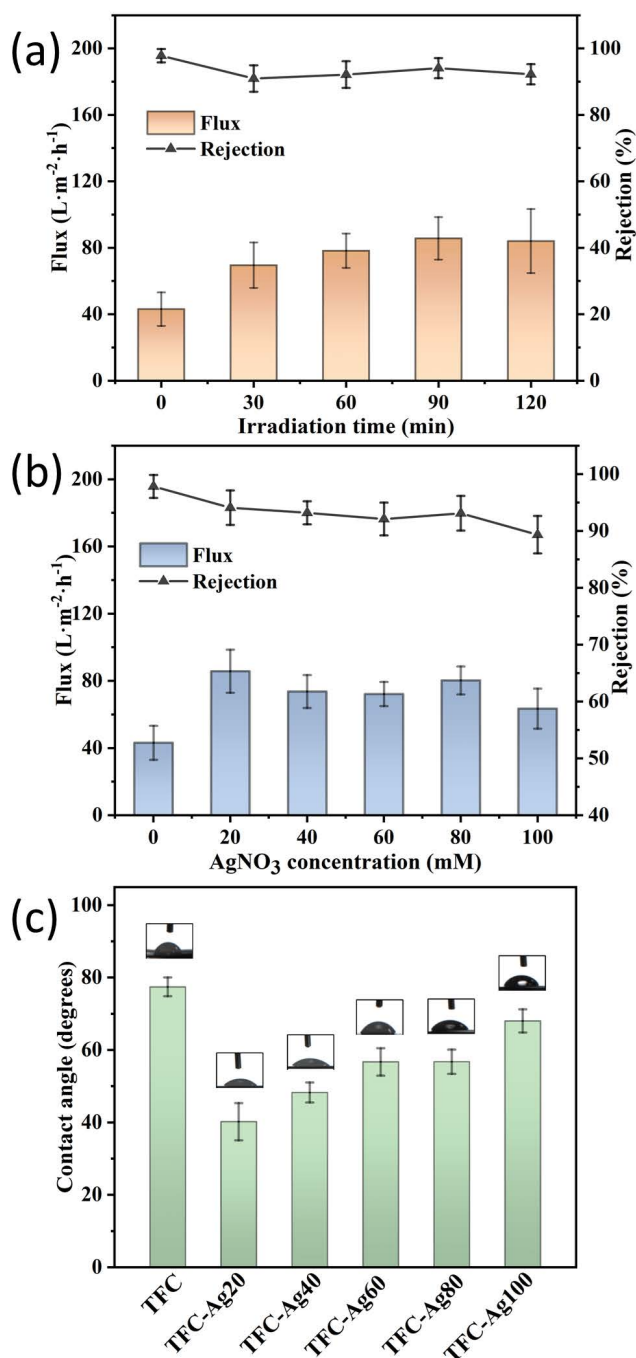


Fig. 5. Effects of UV irradiation time (a) and $AgNO_3$ concentration (b) on the water flux and Na_2SO_4 rejection performance of TFC-Ag membrane; (c) effect of $AgNO_3$ solution concentration on the contact angle of TFC-Ag membrane.

membrane, respectively. After treated by the TFC membrane, there were still a large number of colonies on solid agar. The number of colonies decreased significantly and the antibacterial efficiency reached 96% with the treatment of TFC-Ag membrane. The inhibition zone experiment shows the same result. An antibacterial circle with a diameter of about 12 mm appeared on solid agar which had been treated by TFC-Ag

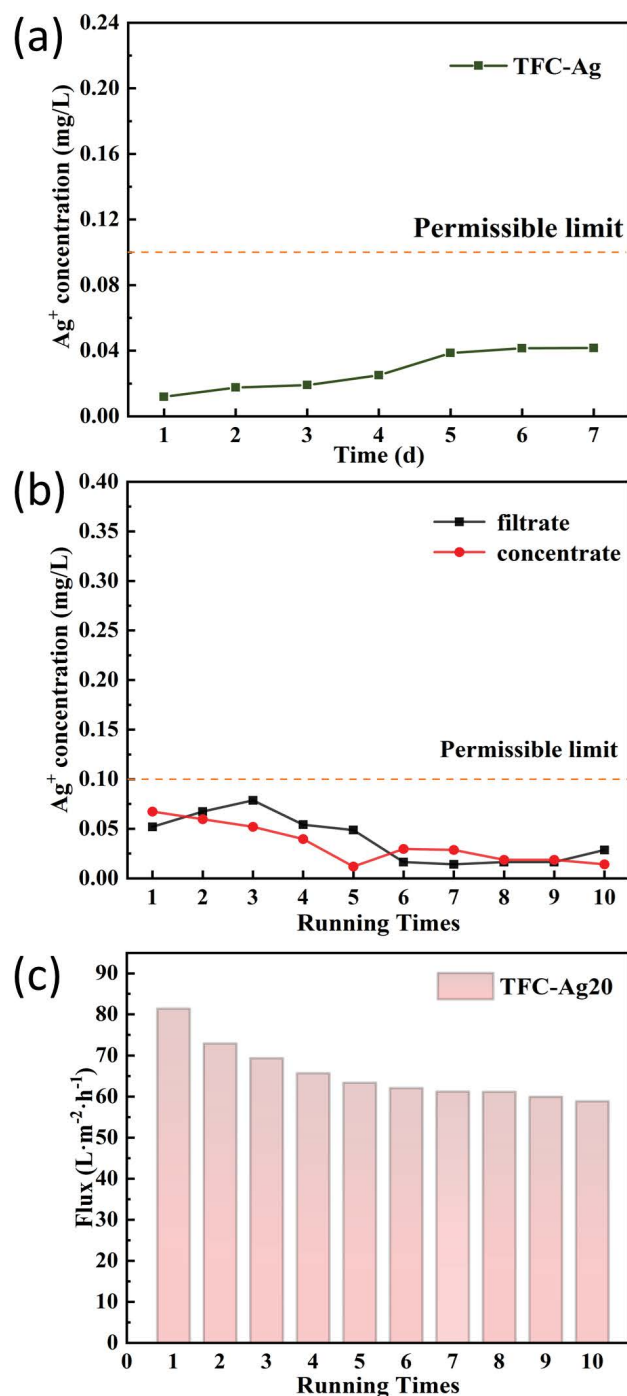


Fig. 6. Release of Ag in the static immersion test (a) and dynamic experiments (b) and (c) pure water flux of the TFC-Ag20 membrane for continuous running cycles.

membrane. These results indicate that TFC-Ag membrane had excellent antibacterial activity due to the presence of Ag nanoparticles [45]. Ag^+ ions could combine with negatively charged proteins and nucleic acids and lead to the changes in cell wall, cell membrane and nucleic acid structure of bacteria. The SEM images (Fig. 7f and g) show the surface morphological change of *E. coli* cell after the contact with TFC-Ag

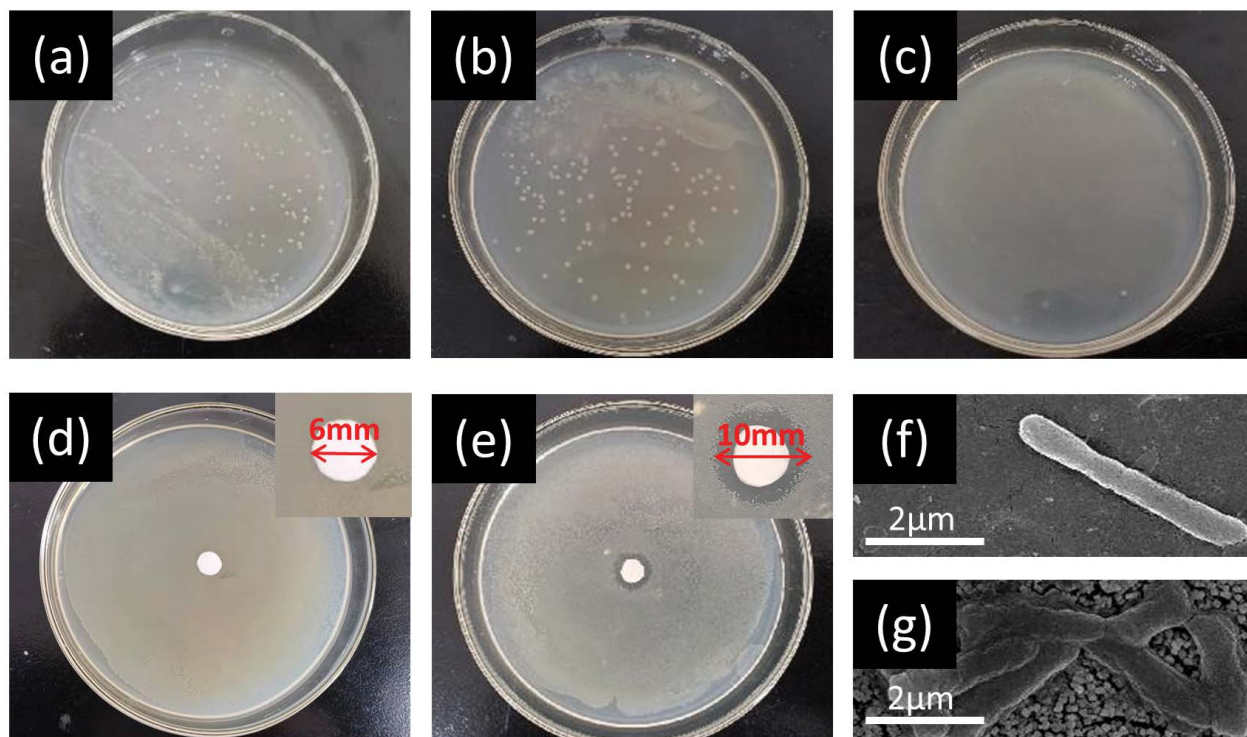


Fig. 7. Optical images of the eluent coated plate after 24 h culture of *E. coli* suspension: (a) blank control, (b) TFC membrane and (c) TFC-Ag membrane. Optical images of *E. coli* inhibition zone: (d) TFC membrane, (e) TFC-Ag membrane. SEM images of *E. coli*: (f) normal and (g) treated by TFC-Ag membrane.

membrane. *E. coli* usually has a smooth rod structure with a complete cell wall (Fig. 7f). The AgNPs in TFC-Ag membrane destroyed the cell wall of bacteria and the destroyed cell wall spread obviously (Fig. 7g).

Three groups of *E. coli* suspension with different concentrations (1.9×10^3 , 1.9×10^4 , 1.9×10^5 CFU/mL) were added in 2,000 ppm Na_2SO_4 solution as feed solution to simulate the bacterial environment in the actual operation process. Fig. 8a shows that the flux attenuation rate of TFC-Ag membrane was significantly less than that of TFC membrane after 18 cycles. The result indicates that the *E. coli* bacteria attached to the surface of the membrane, and blocked the water transfer channel and led to the attenuation of the water flux. Due to the bactericidal effect of silver, the presence of AgNPs could weaken the adverse influence of living *E. coli* bacteria on the performance of membrane.

In addition to biofouling caused by microorganisms, contaminants in water could also produce fouling on the surface or in the structure of membrane [46]. BSA was chosen to analyze the antifouling performance of the TFC-Ag membrane. The flux of the TFC and TFC-Ag membranes for the three cycles is depicted in Fig. 8b. For the DI water filtration, the average water flux of the TFC and TFC-Ag membrane are 45.65 and 83.35 L/m²·h, respectively. When DI water was replaced with BSA solution, the flux of the TFC and TFC-Ag membrane decreased to 15.80 and 24.93 L/m²·h, and the flux attenuation rates are 65.39% and 70.09%, respectively. The flux reduction was due to the contamination of BSA on the membrane surface. When the membrane sample was backwashed by DI water for 30 min, the flux of

membrane would be recovered to some extent. As shown in Fig. 8b, the water flux of the TFC and TFC-Ag membrane recovered to 23.88 and 60.42 L/m²·h, and the flux recovery rates were 55.31% and 72.49%, respectively. Compared with the TFC membrane, the TFC-Ag membrane had better flux recovery rate and anti-pollution performance. The introduction of AgNPs enhanced the hydrophilicity and changed the surface roughness of membrane, thereby enhancing the anti-fouling performance of the TFC-Ag membrane.

Table 1 presents the parameters of membrane filtration resistance and the flux recovery rates in BSA pollution test. The membrane resistance parameters calculated by the resistance model (Text S2) show that R_m reduced from $1.76 \times 10^{12} \text{ m}^{-1}$ to $0.82 \times 10^{12} \text{ m}^{-1}$, and R_p also decreased from $1.61 \times 10^{12} \text{ m}^{-1}$ to $0.31 \times 10^{12} \text{ m}^{-1}$, as AgNPs were introduced to the TFC membrane. The results of TEM revealed that the size of AgNPs in the TFC-Ag membrane was mostly less than 24 nm, therefore AgNPs would not affect the water transport channel in the membrane. Under the combination effects of the AgNPs and the hydrophilic groups of the active layer, the TFC-Ag membrane exhibited benign anti-fouling performance.

4. Conclusions

In this study, TFC-Ag membranes with excellent water flux and anti-biofouling performance were fabricated by a novel photoreduction method. Under the UV irradiation ($\lambda = 365 \text{ nm}$), AgNPs were produced by reducing Ag^+ ions onto TFC membranes, meanwhile the active layer was

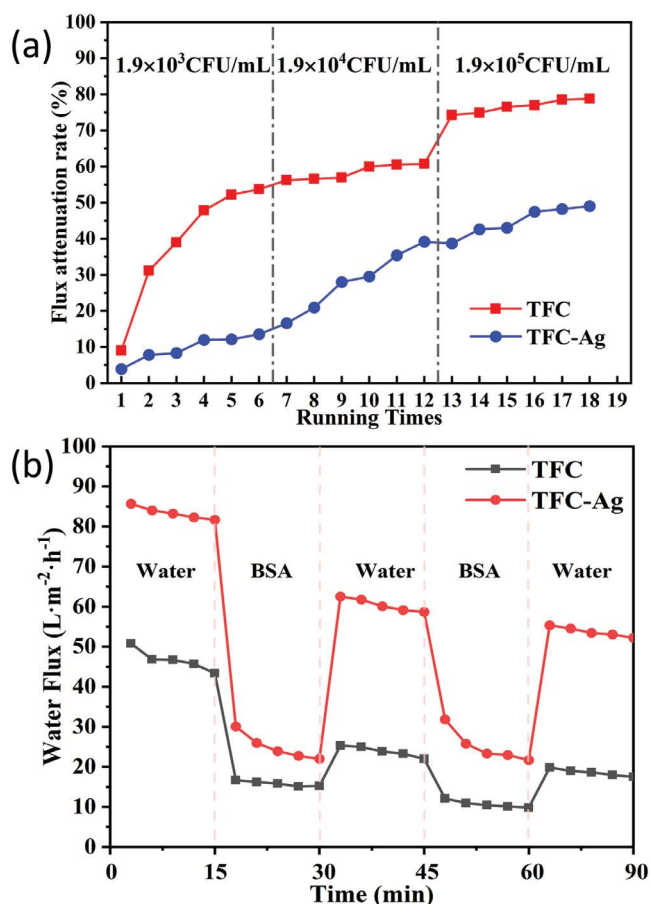


Fig. 8. (a) Flux attenuation of the TFC and TFC-Ag membranes in *E. coli* bacteria suspension of different concentrations and (b) recovery performance of flux for the TFC and TFC-Ag membranes in 3 cycles.

Table 1
Resistance and fouling parameters of membranes^a

	TFC	TFC-Ag20
R_m ($\times 10^{12} \text{ m}^{-1}$)	1.76	0.82
$R_m + R_p$ ($\times 10^{12} \text{ m}^{-1}$)	3.37	1.13
R_p ($\times 10^{12} \text{ m}^{-1}$)	1.61	0.31
DR_i (%)	65.39	70.09
FRR (%)	52.31	72.49

^a R_m : intrinsic resistance of the clean membrane; R_p : fouling resistance; DR_i : flux attenuation rate; FRR: flux recovery ratio.

oxidized. The incorporated AgNPs enhanced the separation and anti-biofouling performance of the TFC-Ag membrane without impairing the TFC membrane structure. The optimal condition for AgNPs preparation was 90 min irradiation time and 20 mM AgNO₃ concentration. The TFC-Ag membrane could achieve an increased water flux of 85.79 L/m²·h, being superior to that of the pristine TFC membrane of 43.15 L/m²·h. The TFC-Ag membrane possessed a larger water flux compared to the previously reported Ag-loaded

nanofiltration membranes. The introduction of AgNPs endowed the TFC-Ag membrane with a long-lasting antibacterial activity against *E. coli* (inhibition efficiency > 90%) and an enhanced anti-biofouling performance. This new photoreduction method provides a facile method to modify the membrane for excellent membrane performance.

Acknowledgements

This work was supported by the National Natural Science Foundation of China (No. 52260010), the scientific start-up fund of Nanchang Hangkong University (EA202102182), and the innovation project from Zhongshan Municipal Science and Technology Bureau (No. 190911162741133, 191021102628332).

References

- [1] R. Zhang, Y. Li, Y. Su, X. Zhao, Y. Liu, X. Fan, T. Ma, Z. Jiang, Engineering amphiphilic nanofiltration membrane surfaces with a multi-defense mechanism for improved antifouling performances, *J. Mater. Chem. A*, 4 (2016) 7892–7902.
- [2] G.S. Lai, W.J. Lau, S.R. Gray, T. Matsuura, R. Jamshidi Gohari, M.N. Subramanian, S.O. Lai, C.S. Ong, A.F. Ismail, D. Emazadah, M. Ghanbari, A practical approach to synthesize polyamide thin film nanocomposite (TFN) membranes with improved separation properties for water/wastewater treatment, *J. Mater. Chem. A*, 4 (2016) 4134–4144.
- [3] X. Song, Q. Zhou, T. Zhang, H. Xu, Z. Wang, Pressure-assisted preparation of graphene oxide quantum dot-incorporated reverse osmosis membranes: antifouling and chlorine resistance potentials, *J. Mater. Chem. A*, 4 (2016) 16896–16905.
- [4] J. Dolina, O. Dlask, T. Lederer, L. Dvořák, Mitigation of membrane biofouling through surface modification with different forms of nanosilver, *Chem. Eng. J.*, 275 (2015) 125–133.
- [5] M. Herzberg, M. Elimelech, Physiology and genetic traits of reverse osmosis membrane biofilms: a case study with *Pseudomonas aeruginosa*, *ISME J.*, 2 (2008) 180–194.
- [6] M. Herzberg, M. Elimelech, Biofouling of reverse osmosis membranes: role of biofilm-enhanced osmotic pressure, *J. Membr. Sci.*, 295 (2007) 11–20.
- [7] D. Seckler, R. Barker, U. Amarasinghe, Water scarcity in the twenty-first century, *Int. J. Water Resour. Dev.*, 15 (1999) 29–42.
- [8] Y. Yang, C. Li, L.-a. Hou, Impact of dead cells on biofouling and pharmaceutically active compounds retention by NF/RO membranes, *Chem. Eng. J.*, 337 (2018) 51–59.
- [9] W. Zhang, D. Guo, Z. Li, L. Shen, R. Li, M. Zhang, Y. Jiao, Y. Xu, H. Lin, A new strategy to accelerate co-deposition of plant polyphenol and amine for fabrication of antibacterial nanofiltration membranes by *in-situ* grown Ag nanoparticles, *Sep. Purif. Technol.*, 280 (2022) 119866, doi: 10.1016/j.seppur.2021.119866.
- [10] Q. Geng, S. Dong, Y. Li, H. Wu, X. Yang, X. Ning, D. Yuan, High-performance photoinduced antimicrobial membrane toward efficient PM_{2.5-0.3} capture and oil-water separation, *Sep. Purif. Technol.*, 284 (2022) 120267, doi: 10.1016/j.seppur.2021.120267.
- [11] X. Guo, D. Liu, T. Han, H. Huang, Q. Yang, C. Zhong, Preparation of thin film nanocomposite membranes with surface modified MOF for high flux organic solvent nanofiltration, *AIChE J.*, 63 (2017) 1303–1312.
- [12] D. Ma, S.B. Peh, G. Han, S.B. Chen, Thin-film nanocomposite (TFN) membranes incorporated with super-hydrophilic metal-organic framework (MOF) UiO-66: toward enhancement of water flux and salt rejection, *ACS Appl. Mater. Interfaces*, 9 (2017) 7523–7534.
- [13] F.-Y. Zhao, Y.-L. Ji, X.-D. Weng, Y.-F. Mi, C.-C. Ye, Q.-F. An, C.-J. Gao, High-flux positively charged nanocomposite nanofiltration membranes filled with poly(dopamine) modified multiwall carbon nanotubes, *ACS Appl. Mater. Interfaces*, 8 (2016) 6693–6700.

- [14] M. Safarpour, V. Vatanpour, A. Khataee, M. Esmaili, Development of a novel high flux and fouling-resistant thin film composite nanofiltration membrane by embedding reduced graphene oxide/TiO₂, *Sep. Purif. Technol.*, 154 (2015) 96–107.
- [15] H. Dong, L. Zhao, L. Zhang, H. Chen, C. Gao, W.S. Winston Ho, High-flux reverse osmosis membranes incorporated with NaY zeolite nanoparticles for brackish water desalination, *J. Membr. Sci.*, 476 (2015) 373–383.
- [16] J. Yin, E.-S. Kim, J. Yang, B. Deng, Fabrication of a novel thin-film nanocomposite (TFN) membrane containing MCM-41 silica nanoparticles (NPs) for water purification, *J. Membr. Sci.*, 423 (2012) 238–246.
- [17] B.-H. Jeong, E.M.V. Hoek, Y. Yan, A. Subramani, X. Huang, G. Hurwitz, A.K. Ghosh, A. Jawor, Interfacial polymerization of thin film nanocomposites: a new concept for reverse osmosis membranes, *J. Membr. Sci.*, 294 (2007) 1–7.
- [18] M. Zhang, K. Zhang, B. De Gussemme, W. Verstraete, Biogenic silver nanoparticles (bio-Ag⁰) decrease biofouling of bio-Ag⁰/PES nanocomposite membranes, *Water Res.*, 46 (2012) 2077–2087.
- [19] E.-S. Kim, G. Hwang, M.G. El-Din, L. Yang, Development of nanosilver and multi-walled carbon nanotubes thin-film nanocomposite membrane for enhanced water treatment, *J. Membr. Sci.*, 394–395 (2012) 37–48.
- [20] A. Mollahosseini, A. Rahimpour, M. Jahamshahi, M. Peyravi, M. Khavarpour, The effect of silver nanoparticle size on performance and antibacteriality of polysulfone ultrafiltration membrane, *Desalination*, 306 (2012) 41–50.
- [21] W.J. Lau, S. Gray, T. Matsuura, D. Emadzadeh, J. Paul Chen, A.F. Ismail, A review on polyamide thin film nanocomposite (TFN) membranes: history, applications, challenges and approaches, *Water Res.*, 80 (2015) 306–324.
- [22] Z. Yang, R. Takagi, X. Zhang, T. Yasui, L. Zhang, H. Matsuyama, Engineering a dual-functional sulfonated polyelectrolyte-silver nanoparticle complex on a polyamide reverse osmosis membrane for robust biofouling mitigation, *J. Membr. Sci.*, 618 (2021) 118757, doi: 10.1016/j.memsci.2020.118757.
- [23] Z. Yang, H. Guo, Z.-k. Yao, Y. Mei, C.Y. Tang, Hydrophilic silver nanoparticles induce selective nanochannels in thin film nanocomposite polyamide membranes, *Environ. Sci. Technol.*, 53 (2019) 5301–5308.
- [24] J.C. Scaiano, K.G. Stamplecoskie, G.L. Hallett-Tapley, Photochemical Norrish type I reaction as a tool for metal nanoparticle synthesis: importance of proton coupled electron transfer, *Chem. Commun.*, 48 (2012) 4798–4808.
- [25] K.G. Stamplecoskie, J.C. Scaiano, Light emitting diode irradiation can control the morphology and optical properties of silver nanoparticles, *J. Am. Chem. Soc.*, 132 (2010) 1825–1827.
- [26] Q. Xie, S. Zhang, Z. Hong, H. Ma, C. Liu, W. Shao, Effects of casting solvents on the morphologies, properties, and performance of polysulfone supports and the resultant graphene oxide-embedded thin-film nanocomposite nanofiltration membranes, *Ind. Eng. Chem. Res.*, 57 (2018) 16464–16475.
- [27] L. Li, S. Zhang, X. Zhang, Preparation and characterization of poly(piperazineamide) composite nanofiltration membrane by interfacial polymerization of 3,3',5,5'-biphenyl tetraacyl chloride and piperazine, *J. Membr. Sci.*, 335 (2009) 133–139.
- [28] Z.Y. Zhang, Y. Kuang, Y. Lin, D.Y. Wu, A closed-loop sustainable scheme for silver recovery from water by reusable thiol-grafted graphene oxide, *J. Cleaner Prod.*, 305 (2021) 127146, doi: 10.1016/j.jclepro.2021.127146.
- [29] S.P. Dubey, M. Lahtinen, M. Sillanpää, Tansy fruit mediated greener synthesis of silver and gold nanoparticles, *Process Biochem.*, 45 (2010) 1065–1071.
- [30] P.F. Andrade, A.F. de Faria, S.R. Oliveira, M.A.Z. Arruda, M. do Carmo Gonçalves, Improved antibacterial activity of nanofiltration polysulfone membranes modified with silver nanoparticles, *Water Res.*, 81 (2015) 333–342.
- [31] C.Y.Y. Tang, Y.-N. Kwon, J.O. Leckie, Effect of membrane chemistry and coating layer on physicochemical properties of thin film composite polyamide RO and NF membranes: I. FTIR and XPS characterization of polyamide and coating layer chemistry, *Desalination*, 242 (2009) 149–167.
- [32] C.L. Liu, Y.X. Sun, Z.B. Chen, S.B. Zhang, From ultrafiltration to nanofiltration: nanofiltration membrane fabricated by a combined process of chemical crosslinking and thermal annealing, *Sep. Purif. Technol.*, 212 (2019) 465–473.
- [33] S. Therias, N.T. Dintcheva, J.-L. Gardette, F.P. La Mantia, Photooxidative behaviour of polyethylene/polyamide-6 blends, *Polym. Degrad. Stab.*, 95 (2010) 522–526.
- [34] N. Hoffmann, Photochemical reactions as key steps in organic synthesis, *Chem. Rev.*, 108 (2008) 1052–1103.
- [35] S.S. Liu, M.Y. Zhang, F. Fang, L. Cui, J.J. Wu, R. Field, K.S. Zhang, Biogenic silver nanocomposite TFC nanofiltration membrane with antifouling properties, *Desal. Water Treat.*, 57 (2016) 10560–10571.
- [36] S.S. Liu, F. Fang, J.J. Wu, K.S. Zhang, The anti-biofouling properties of thin-film composite nanofiltration membranes grafted with biogenic silver nanoparticles, *Desalination*, 375 (2015) 121–128.
- [37] X. Wu, F. Fang, B.F. Zhang, J.J. Wu, K.S. Zhang, Biogenic silver nanoparticles-modified forward osmosis membranes with mitigated internal concentration polarization and enhanced antibacterial properties, *npj Clean Water*, 5 (2022) 41, doi: 10.1038/s41545-022-00190-1.
- [38] N. Ahmad, A. Samavati, N.A.H.M. Nordin, J. Jaafar, A.F. Ismail, N.A.N.N. Malek, Enhanced performance and antibacterial properties of amine-functionalized ZIF-8-decorated GO for ultrafiltration membrane, *Sep. Purif. Technol.*, 239 (2020) 116554, doi: 10.1016/j.seppur.2020.116554.
- [39] Z. Liang, J. Wang, Q. Zhang, T. Zhuang, C. Zhao, Y. Fu, Y. Zhang, F. Yang, Composite PVDF ultrafiltration membrane tailored by sandwich-like GO@UiO-66 nanoparticles for breaking the trade-off between permeability and selectivity, *Sep. Purif. Technol.*, 276 (2021) 119308, doi: 10.1016/j.seppur.2021.119308.
- [40] Z. Yang, Y.C. Wu, H. Guo, X.H. Ma, C.E. Lin, Y. Zhou, B. Cao, B.K. Zhu, K.M. Shih, C.Y.Y. Tang, A novel thin-film nano-templated composite membrane with *in-situ* silver nanoparticles loading: separation performance enhancement and implications, *J. Membr. Sci.*, 544 (2017) 351–358.
- [41] S.Y. Lee, H.J. Kim, R. Patel, S.J. Im, J.H. Kim, B.R. Min, Silver nanoparticles immobilized on thin film composite polyamide membrane: characterization, nanofiltration, antifouling properties, *Polym. Adv. Technol.*, 18 (2007) 562–568.
- [42] S.H. Park, Y.S. Ko, S.J. Park, J.S. Lee, J. Cho, K.Y. Baek, I.T. Kim, K. Woo, J.H. Lee, Immobilization of silver nanoparticle-decorated silica particles on polyamide thin film composite membranes for antibacterial properties, *J. Membr. Sci.*, 499 (2016) 80–91.
- [43] H.O. World, Guidelines for Drinking-Water Quality, World Health Organization, Geneva, Switzerland, 2004.
- [44] S. Jeon, J.-H. Lee, Rationally designed *in-situ* fabrication of thin film nanocomposite membranes with enhanced desalination and anti-biofouling performance, *J. Membr. Sci.*, 615 (2020) 118542, doi: 10.1016/j.memsci.2020.118542.
- [45] C. Zhang, Z. Hu, B. Deng, Silver nanoparticles in aquatic environments: physicochemical behavior and antimicrobial mechanisms, *Water Res.*, 88 (2016) 403–427.
- [46] L. Wang, W. Wang, N. Graham, M.S. Siddique, H. Yang, W. Yu, Copper doped Fe-N-C as an excellent Fenton-like catalyst for membrane fouling mitigation against natural organic matters at neutral pH, *J. Cleaner Prod.*, 335 (2022) 130368, doi: 10.1016/j.jclepro.2022.130368.

Supporting information

S1. Analytical method for Ag⁺ concentration

First, 1 mL of sodium citrate solution (50 g/L) and 1 drop of methyl orange solution (1 g/L) were added into a 25 mL flask. Then, suitable sodium hydroxide solution (1 mol/L) was added in the flask until the solution color changed from red to yellow. Afterwards, 2 mL of acetic acid-sodium acetate buffer solution (1 mol/L, pH = 5), 2 mL of EDTA-2Na

solution (0.1 mol/L), 2 mL of sodium lauryl sulfate solution (10 g/L), and 2 mL of 3,5-BR₂-PADAP ethanol solution (0.25 g/L) were successively added and mixed efficiently. The obtained solution was diluted and the final solution volume was 25 mL. The Ag⁺ content was measured by detecting the absorbance at 570 nm of the final solution.

S2. Membrane resistance parameter calculation

The used resistance model for the calculation of membrane resistance parameters is illustrated as Eq. (S1). Firstly, the clean membrane was used for pure water permeation experiment to control R_p and R_{cp} at 0. Thus, Eq. (S1) could be transformed to Eq. (S2) and the R_m was obtained. Secondly, the membrane was utilized to remove Bovine Serum Albumin protein (BSA) from solution. After that, the polluted membrane was backwashed for the next pure water permeation. In this case, the concentration polarization induced boundary layer of membrane was thought to be removed and led to the 0 value of R_{cp} . Therefore, Eq. (S1) could be transformed to Eq. (S3) and the R_p value was acquired. Then, DR_i and FRR could be calculated according to Eqs. (4) and (5), respectively.

$$J = \frac{\Delta P}{\mu(R_m + R_p + R_{cp})} \quad (S1)$$

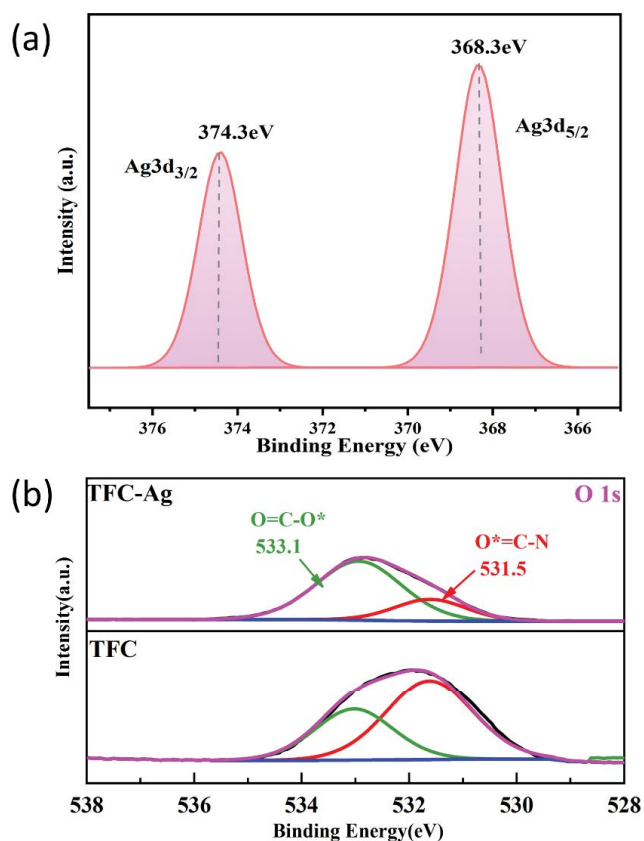


Fig. S1. (a) Ag 3d and (b) O 1s XPS spectra of the TFC and TFC-Ag membranes.

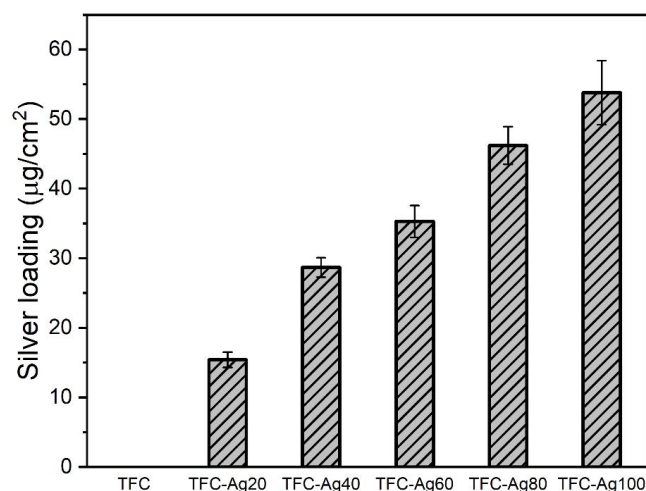


Fig. S2. Ag loading amounts for the prepared TFC-Ag membranes.

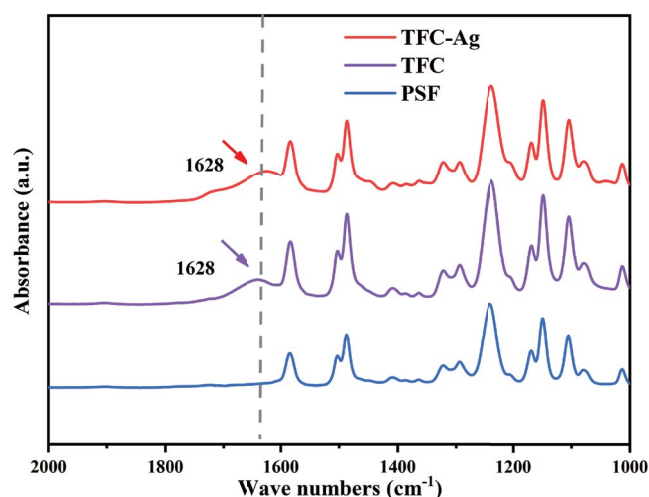


Fig. S3. FTIR spectra of the PSF, TFC and TFC-Ag membranes. The adsorption band at 1,628 cm⁻¹ is attributed to the stretching vibration of C=O in the polyamide separation layer, suggesting the successful construction of nanofiltration membrane.

$$J_{w1} = \frac{\Delta P}{\mu R_m} \quad (S2)$$

$$J_{w2} = \frac{\Delta P}{\mu(R_m + R_p)} \quad (S3)$$

$$DR_i (\%) = \left(1 - \frac{J_{pl}}{J_{w1}}\right) \times 100\% \quad (S4)$$

$$FRR (\%) = \frac{J_{w2}}{J_{w1}} \times 100\% \quad (S5)$$

where J is the membrane permeation flux ($L/m^2 \cdot h$); J_{w1} the pure water flux of the clean membrane; J_{w2} the pure water flux of the backwashed membrane; J_{p1} the BSA solution flux ($L/m^2 \cdot h$); ΔP the pressure gap between the top and bottom surfaces of membrane (Pa); μ the solution viscosity (Pa·s);

R_m the intrinsic resistance of the clean membrane (m^{-1}); R_p the fouling resistance (m^{-1}); R_{cp} the boundary layer resistance induced by concentration polarization (m^{-1}); DR_t the flux attenuation rate (%); FRR the flux recovery ratio (%).